Acta Crystallographica Section D
**Biological Crystallography**
ISSN 0907-4449

# Crystallographic determination of the disease-associated T1184R variant of complement regulator factor H

**Hugh P. Morgan,[a] Jingzi Jiang,[a] Andrew P. Herbert,[b]‡ David Kavanagh,[c] Dušan Uhrin,[b] Paul N. Barlow[b] and Jonathan P. Hannan[a]***

[a]Institute of Structural and Molecular Biology, School of Biological Sciences, University of Edinburgh, King's Buildings, Mayfield Road, Edinburgh EH9 3JR, Scotland, [b]Edinburgh Biomolecular NMR Unit, EaStCHEM, School of Chemistry, University of Edinburgh, Edinburgh EH9 3JJ, Scotland, and [c]The Institute of Human Genetics, University of Newcastle upon Tyne, Newcastle upon Tyne NE1 3BZ, England

‡ Present address: The Physiological Laboratory, School of Biomedical Sciences, Crown Street, University of Liverpool, Liverpool L69 3BX, England.

Correspondence e-mail: jonathan.hannan@ed.ac.uk

Received 25 March 2011
Accepted 24 April 2011

**PDB Reference:** T1184R variant of complement regulator factor H, 3r62.

The soluble 155 kDa glycoprotein factor H (FH) protects host tissue from damage by the human complement system. It accelerates decay of the alternative-pathway C3 convertase, C3bBb, and is a cofactor for factor I-mediated cleavage of the opsonin C3b. Numerous mutations and single-nucleotide polymorphisms (SNPs) occur in the gene encoding FH and the resulting missense mutations and truncation products result in altered functionality that predisposes to the development of the serious renal condition atypical haemolytic uraemic syndrome (aHUS). Other polymorphisms are linked to membranoproliferative glomerulonephritis and macular degeneration. The two C-terminal modules of FH (FH19-20) harbour numerous aHUS-associated mutations that disrupt the ability of factor H to protect host cells from complement-mediated damage. In this work, the crystal structure of an aHUS-associated T1184R variant of FH19-20 at a resolution of 1.52 Å is described. It is shown that this mutation has negligible structural effects but causes a significant change in the electrostatic surface of these two domains. Mechanisms are discussed by which this mutation may alter FH–ligand interactions, particularly with regard to the extension of a region of this molecule within module 20 that has been associated with the binding of glycosaminoglycans (GAGs) or sialic acid residues.

## 1. Introduction

Complement factor H (FH) plays an essential role in the regulation of the alternative pathway of complement by preventing the amplification of the activation-specific C3 fragment, C3b, on self-surfaces. Mutations and SNPs in the FH gene are linked to diseases of the eye and kidney caused by an overactive complement system (reviewed in de Córboba & de Jorge, 2008). FH is an abundant 155 kDa soluble glycoprotein comprising 20 tandemly arranged complement control protein modules (CCPs). These compact modules each comprise approximately 60 amino-acid residues and occur widely amongst the regulators of complement activation (RCA) family of proteins. FH acts as a cofactor for complement factor I (FI) that proteolytically cleaves C3b to its inactive form iC3b. FH also prevents the formation, and accelerates the decay, of the alternative-pathway convertase complex consisting of C3b and Bb (C3bBb; Whaley & Ruddy, 1976; Weiler *et al.*, 1976; Pangburn *et al.*, 1977) that otherwise enzymatically cleaves C3 to generate more C3b (an opsonin) and C3a (an anaphylatoxin). FH binds very effectively to C3b and C3bBb, which are associated with self-surfaces (as opposed to foreign surfaces), since it recognizes a composite binding site formed by C3b

and specific polyanionic markers such as glycosaminoglycans and sialic acid (Meri & Pangburn, 1994; Pangburn, 2000). Crucially, FH does not bind efficiently to, nor protect from complement, foreign surfaces that lack such markers (Pangburn, 2000). FH is therefore integral to the ability of the innate immune response to discriminate between host cells and pathogens.

Two regions of FH interact cooperatively with C3b: the amino-terminal four CCP modules (FH1-4) and the two carboxyl-terminal CCP modules (FH19-20) (Gordon *et al.*, 1995; Pangburn, 2002; Schmidt *et al.*, 2008; Sharma & Pangburn, 1996). High-resolution crystallographic data have been obtained for these two primary contact sites in the forms of FH1-4–C3b and FH19-20–C3d complexes (Wu *et al.*, 2009; Kajander *et al.*, 2011; Morgan et al., 2011). These two terminal regions of FH clamp onto C3b, with the intervening 14 CCP modules of the molecule adopting a loop-like arrangement. The CCP19-20 site additionally binds *via* CCP20 to surface

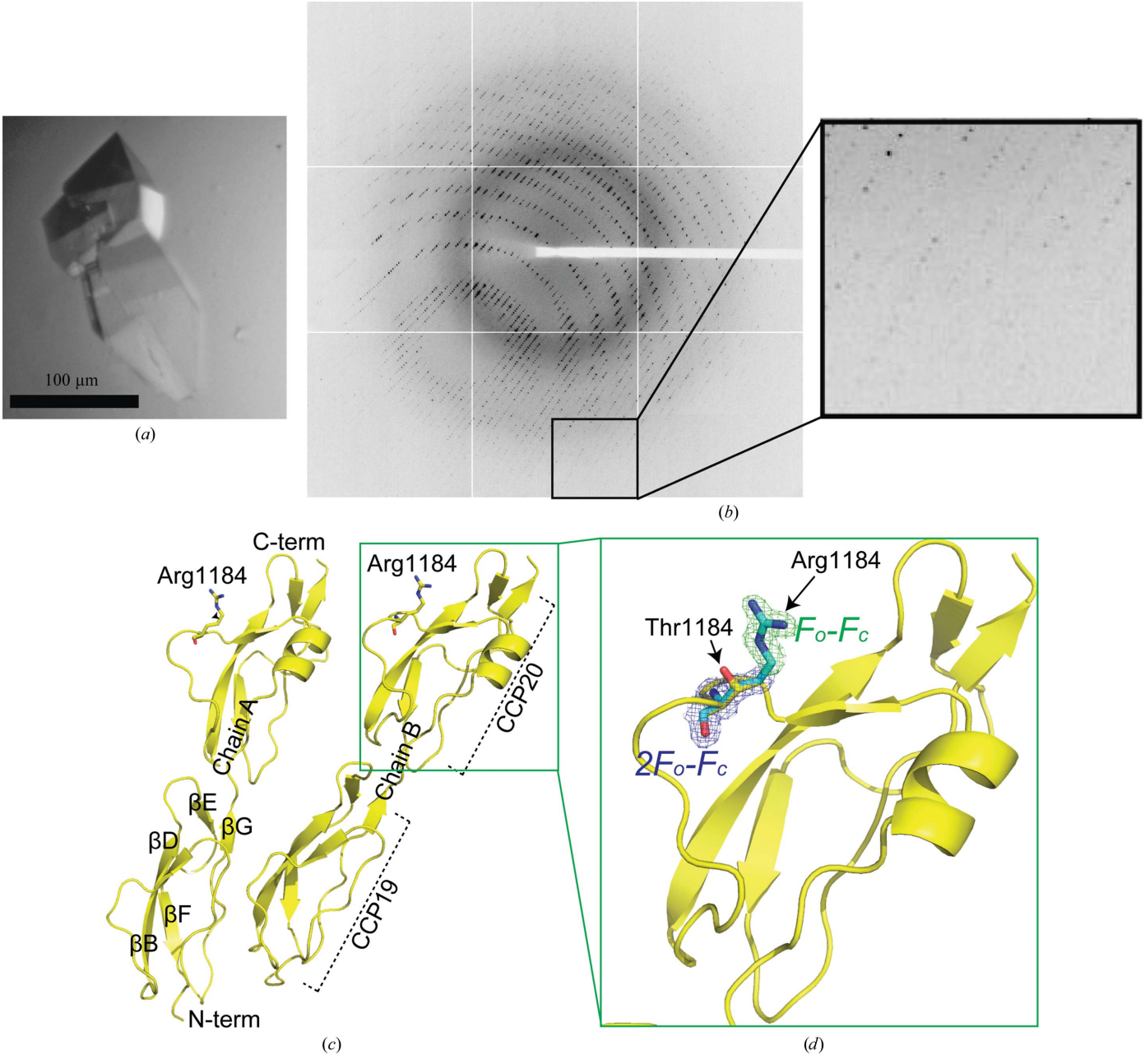


**Figure 1**
(*a*) Crystals of T1184R FH19-20. (*b*) A representative X-ray diffraction image from a T1184R FH19-20 crystal. The edge of the detector corresponds to a resolution of 1.27 Å. (*c*) A cartoon representation of the asymmetric unit of the FH19-20 T1184R X-ray crystal structure comprising two individual monomers (PDB entry 3r62). $\beta$-Strands $\beta$B and $\beta$D and the early part of the loop between $\beta$D and $\beta$E of CCP19 comprise the majority of the binding interface between the C-terminus of FH and C3b. (*d*) An OMIT map highlighting the Thr1184-to-Arg mutation. The resolution of the electron density ($2F_o - F_c$ map shown in blue) map is 1.52 Å and is contoured at 1$\sigma$. The OMIT map shown was calculated by refining Thr1184 in place of Arg. Clear $F_o - F_c$ density (green) is observed for the arginine side chain.

polyanions, thus contributing crucially to self-tissue recognition (Morgan *et al.*, 2011; Schmidt *et al.*, 2008; Kajander *et al.*, 2011). An additional polyanion-binding site occurs on CCP7 (Blackmore *et al.*, 1996, 1998; Pangburn *et al.*, 1991; Herbert *et al.*, 2007; Morgan *et al.*, 2011).

Haemolytic uraemic syndrome (HUS), which is characterized by thrombocytopenia, microangiopathic haemolytic anaemia and renal failure, is classified as either diarrhoeal-associated or non-diarrhoeal/atypical HUS (aHUS). The former, accounting for more than 90% of cases, is commonly a sequela of *Escherichia coli* O57:H7 infections, but aHUS is not infection-related and has a much poorer prognosis. Environmental and genetic risk factors that have been linked to the pathogenesis of aHUS include numerous mutations in FH as well as other complement proteins involved in the alternative pathway (reviewed in Kavanagh *et al.*, 2006; de Córdoba & de Jorge, 2008). The C3b-binding and polyanion-recognition CCP19-20 region of FH is a hotspot for missense mutations that predispose to aHUS (Zipfel *et al.*, 1999; Warwicker *et al.*, 1998; Venables *et al.*, 2006; Richards *et al.*, 2001; Caprioli *et al.*, 2003) and has been subjected to intense structural and functional analysis. In this study, we report the three-dimensional structure of an aHUS-associated T1184R form of FH CCP19-20 (FH19-20) at 1.52 Å resolution. We discuss our structure in the context of functional data for the T1184R mutant, structural knowledge concerning the FH–C3b and FH–GAG interactions, and a putative FH–C3d interaction.

## 2. Materials and methods

### 2.1. Protein production and crystallization

Recombinant T1184R FH19-20 was produced and purified as previously described (Ferreira *et al.*, 2009; Herbert *et al.*, 2006). Briefly, DNA encoding the fragment containing human FH residues 1107–1231 (native sequence numbering) was cloned into the *Pichia pastoris* expression vector pPICZ$\alpha$. A QuikChange site-directed mutagenesis kit (Stratagene) was employed to generate a threonine-to-arginine substitution at position 1184 according to the manufacturer's instructions. This T1184R mutation has been associated with the development of aHUS (Kavanagh *et al.*, 2006). Plasmid DNA containing the T1184R-modified FH19-20 insert was subsequently used to transform a *P. pastoris* expression host. The resulting recombinant T1184R FH19-20 was secreted into the medium and then purified by cation-exchange chromatography. The purified recombinant T1184R FH19-20 protein contains an additional four-residue cloning artefact (EAEF) at the N-terminus. Successful introduction of the single-site mutation was confirmed by mass spectroscopy (not shown).

Crystals of T1184R FH19-20 were grown at 290 K by the vapour-diffusion method from hanging drops. The drops consisted of equal volumes of protein solution concentrated to 6.6 mg ml$^{-1}$ in phosphate-buffered saline pH 7.4 (containing 137 m*M* NaCl, 8.1 m*M* $Na_2HPO_4$, 2.7 m*M* KCl, 1.5 m*M* $KH_2PO_4$), 5 m*M* EDTA and 0.005%(*w*/*v*) sodium azide and well solution consisting of 0.1 *M* Tris–HCl pH 8.5 and 12% polyethylene glycol 8000 as the precipitant. Crystals grew after approximately two weeks (Fig. 1*a*). Crystals were flash-frozen in liquid nitrogen after successive soaks in cryoprotectant solutions containing 10 and 25%(*v*/*v*) glycerol.

**Table 1**
Data-collection and refinement statistics.

Values in parentheses are for the highest resolution shell.

| | |
|---|---|
| Data collection | |
| Space group | $P2_12_12_1$ |
| Unit-cell parameters (Å) | $a$ = 36.89, $b$ = 52.84, $c$ = 142.63 |
| Resolution (Å) | 1.52 |
| $R_{merge}$ (%) | 10.9 (68.1) |
| $R_{meas}$ (%) | 11.8 (76.9) |
| $\langle I/\sigma(I)\rangle$ | 11.5 (2.1) |
| Completeness (%) | 99.6 (95.6) |
| Multiplicity | 6.5 (4.6) |
| Wilson $B$ factor (Å$^2$) | 24.23 |
| Average mosaicity (°) | 0.60 |
| Refinement | |
| Resolution (Å) | 42.46–1.52 |
| No. of reflections | 41260 |
| $R_{work}/R_{free}$ | 17.78/20.80 |
| No. of atoms | |
| Protein | 2175 |
| Ligand (glycerol) | 6 |
| Water | 398 |
| Average protein $B$ factors (Å$^2$) | |
| Protein | 16.80 |
| Ligand | 32.12 |
| Water | 30.47 |
| R.m.s. deviations | |
| Bond lengths (Å) | 0.03 |
| Bond angles (°) | 2.37 |

### 2.2. Data collection and structure determination

Diffraction data were measured on beamline I03 of the Diamond Light Source using an ADSC Q315 CCD detector (Fig. 1*b*) and a crystal-to-detector distance of 219 mm. A total of 60 images were collected over 180° with an exposure time of 0.25 s at 50% attenuation. Data were indexed with *MOSFLM* and merged and scaled with *SCALA*. The structure of the T1184R variant of FH19-20 was solved by molecular replacement using the program *Phaser* (McCoy *et al.*, 2007), with the previously determined NMR structure (PDB entry 2bzm; Herbert *et al.*, 2006) as a search model. There was a clear molecular-replacement solution with two monomers in the crystallographic asymmetric unit. The initial model was subjected to ten cycles of restrained refinement using the program *REFMAC* (Murshudov *et al.*, 2011), resulting in $R$ and $R_{free}$ values of 31.85 and 35.06, respectively. Using the program *Coot* (Emsley & Cowtan, 2004), Thr1184 was mutated to Arg1184, for which clear $F_o - F_c$ electron density was observed, alternative side-chain conformers were constructed and the additional residues were added to the N-terminus. The model was then subjected to several rounds of restrained refinement, resulting in $R$ and $R_{free}$ values of 26.75 and 30.34, respectively. Water molecules were added to the model using *Coot*. Water molecules were accepted based on the following criteria: no less than a 3.2$\sigma$ peak height in the difference maps, hydrogen-bonding distances to protein atoms of between 2.0 and 3.5 Å and a $B$ factor of less than 55 Å$^2$.

Areas of disorder were carefully modelled into $F_o - F_c$ electron density and the changes in the $R$ and $R_{free}$ values were used to assess the final model quality. This resulted in a final model of 248 residues, composed of two T1184R FH19-20 molecules (molecule 1/chain $A$ = Gly1107–Arg1231, molecule 2/chain $B$ = Glu1105–Arg1231), and 398 water molecules. The $R$ and $R_{free}$ values converged after 20 cycles of *REFMAC* at 17.78 and 20.80, respectively. Data-reduction and refinement statistics are summarized in Table 1.

### 2.3. Validation and deposition

The geometry of the model was assessed using *MolProbity* (Chen *et al.*, 2010) and quaternary-structure analysis was performed using the *PISA* server (Krissinel & Henrick, 2007). Atomic coordinates and the experimental structure factors for the 1.52 Å structure of the T1184R FH19-20 variant have been deposited in the Protein Data Bank with code 3r62.

## 3. Results and discussion

The structure of the T1184R aHUS-associated variant of FH19-20 was successfully determined at a resolution of 1.52 Å (Figs. 1*c* and 1*d*). The crystal structure was solved by molecular replacement using the NMR structure of wild-type FH19-20 as the search model (PDB entry 2bzm; Herbert *et al.*, 2006). The orthorhombic crystal form contained two protein molecules in the asymmetric unit, with a solvent content of 47%. The overall architecture is similar to that previously reported for wild-type FH19-20 (Jokiranta *et al.*, 2006; Herbert *et al.*, 2006) and to those of two other single-site mutants of FH19-20 for which structures have been determined by crystallography: Q1139A, which is located within module 19, determined at 1.65 Å and R1203S, which is located within module 20, determined at 2.0 Å (Bhattacharjee *et al.*, 2010). With the exception of the NMR solution structure (Herbert *et al.*, 2006), all of these FH19-20 molecules have been crystallized as tetrameric assemblies (wild-type FH19-20, PDB entry 2g7i, Jokiranta *et al.*, 2006; Q1139A, PDB entry 3kzv, Bhattacharjee *et al.*, 2010; R1203A, PDB entry 3kzj, Bhattacharjee *et al.*, 2010) and indeed, a potential physiological role for oligomerization has been suggested previously (Jokiranta *et al.*, 2006). In comparison, in our study two near-identical molecules of T1184R FH19-20 are observed in the asymmetric unit, forming a dimer that is stabilized by contacts between residues within CCP19 of the respective FH molecules. In particular, residues Asp1116, Glu1159, Asp1162, Cys1163, His1165 and Asp1220 from chain *A*, and Ser1122, Ser1133, Glu1135, Lys1148, Arg1149, Thr1151 and Arg1153 from chain *B* are involved in the formation of intermolecular hydrogen bonds and salt bridges. Analysis and scoring of this dimer interface using the program *PISA* (Krissinel & Henrick, 2007) indicates that FH19-20 dimerization is likely to be the result of crystal packing. Accordingly, the dimer interface observed in this structural elucidation is not likely to be physiologically relevant to the regu-

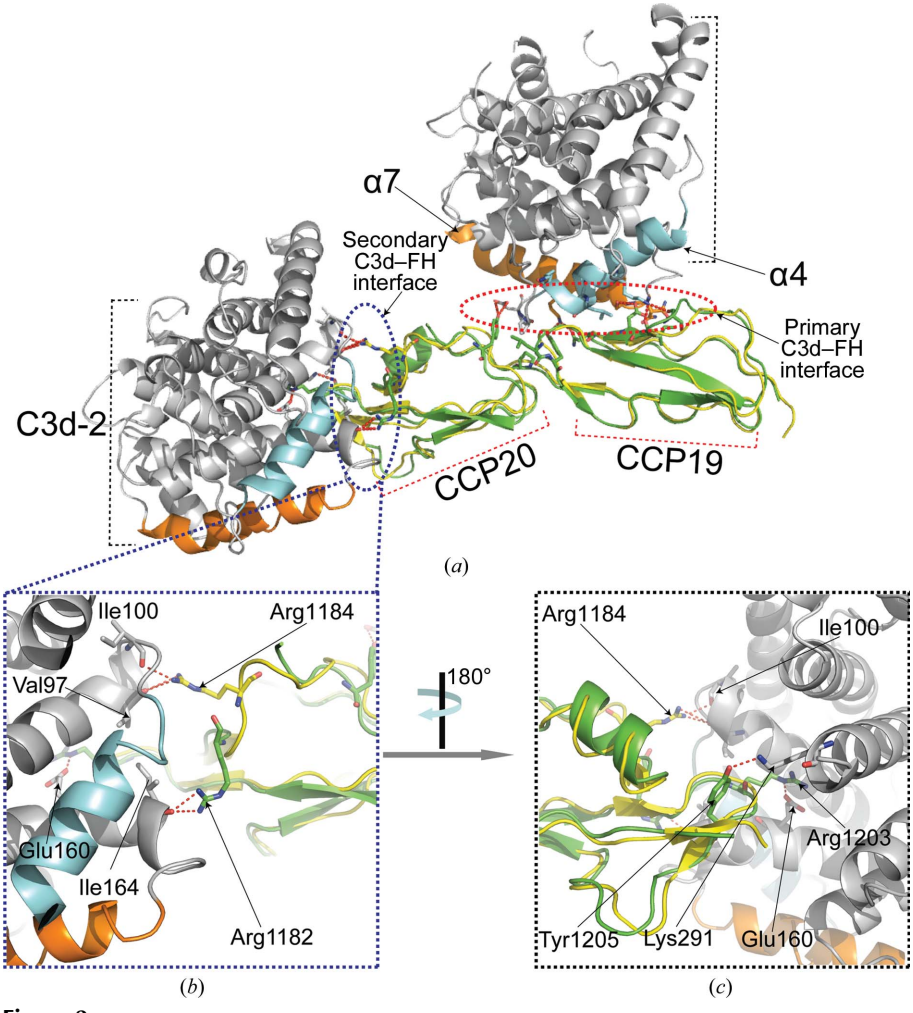


**Figure 2**
(*a*) A superimposition of the T1184R FH19-20 (yellow) structure with wild-type FH19-20 (green) belonging to the C3d–wild-type FH19-20 complex (determined at 2.1 Å resolution; PDB entry 3oxu; Morgan *et al.*, 2011). Amino acids belonging to two interacting helices α7 (orange; residues 170–189) and α4 (cyan; residues 103–119) of C3d-1 (which is shown in grey) form the majority of the interactions with FH (which extrapolates to the C3b–FH19-20 interface), predominantly interacting with module 19. An additional C3d molecule (C3d-2) binds to a putative secondary site (as proposed by Kajander *et al.*, 2011) located on module 20 of FH. The heterotrimer shown was generated using the wild-type C3d–FH19-20 complex (Morgan *et al.*, 2011). (*b*, *c*) Two enlarged views of the secondary C3d–FH19-20 interface. The T1184R mutation is unlikely to directly affect C3b binding at the primary site as it occurs towards the C-terminal region of module 20, but it is close to a putative secondary C3d-binding site. Potential hydrogen bonds (shown as dashed red lines) between Arg1184 and the carbonyl O atom of Ile100 and Val97 are shown.

lation of complement on self-surfaces. These data are in accordance with previously reported analytical ultracentrifugation studies, which demonstrate that full-length FH (CCP1-20) is monomeric under solution conditions (Aslam & Perkins, 2001).

In a previous study reporting the link between the missense T1184R mutation and the development of aHUS, levels of circulating FH were reported to be normal in a sporadic patient (Richards *et al.*, 2001). Accordingly, any differences in host-cell recognition by FH or regulation of complement by FH should be attributed to structural or functional perturbations resulting from the threonine-to-arginine substitution rather than to altered levels of expression. In our structure of the T1184R variant of FH19-20 each monomer adopts a rod-like structure in which the two CCP modules are aligned in an end-to-end manner. Thus, the crystal structure reveals that neither the intermodular orientation nor the global fold of CCP20 are perturbed by this mutation. Indeed, the structures of the wild-type and T1184R forms of FH19-20 may be superimposed (backbone atoms) with an r.m.s.d. of 1.03 Å (T1184R, PDB entry 3r62, chain *A*; FH19-20, PDB entry 3oxu, chain *F*, Morgan *et al.*, 2011) (Fig. 2). Structural changes are thus highly localized to the immediate vicinity of the mutated side chain. On the other hand, the gain of a positive charge in

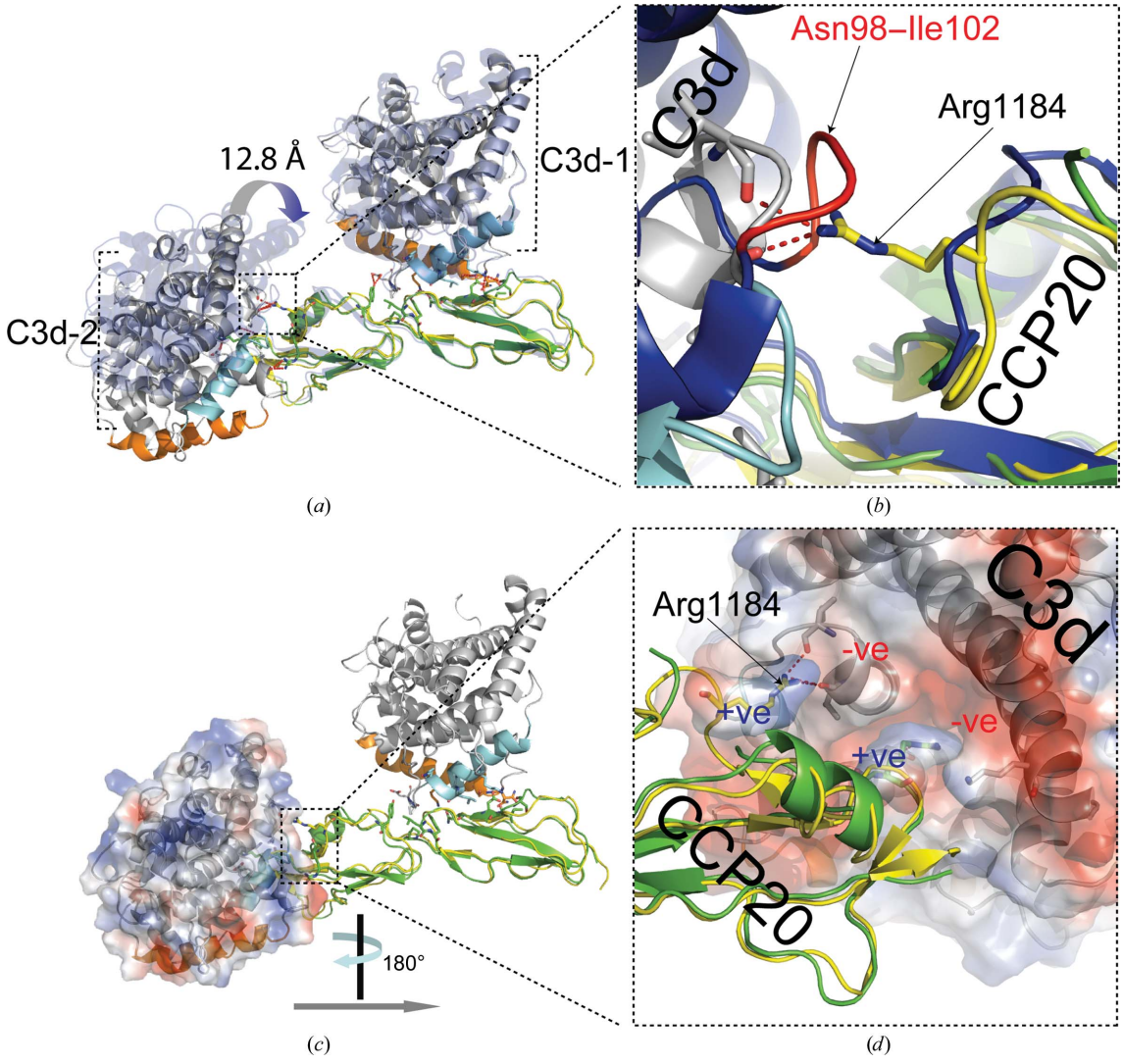


**Figure 3**
(*a*) A superposition of T1184R FH19-20 (yellow) with wild-type FH19-20 (green) belonging to the C3d–wild-type FH19-20 heterotrimer (PDB entry 3oxu; Morgan *et al.*, 2011) and D1119G/Q1139A FH19-20 belonging to the C3d–D1119G/Q1139A FH19-20 heterotrimer (determined at 2.3 Å resolution; PDB entry 2xqw; Kajander *et al.*, 2011; shown in faded blue). The C3d–wild-type FH19-20 heterotrimer is coloured identically to that shown in Fig. 2. C3d-2 belonging to the C3d–D1119G/Q1139A FH19-20 complex, although making similar interactions with FH (Figs. 2*b* and 2*c*), is swivelled 12.8 Å (measured between the carbonyl O atom of Glu47) towards C3d-1 (as indicated by the arrow). (*b*) Arg1184 belonging to T1184R FH19-20 sterically clashes with C3d-2 (specifically residues Asn98–Ile102) when superposed onto the structure of D1119G/Q1139A FH19-20 (belonging to the C3d–D1119G/Q1139A FH19-20 heterotrimer). (*c*) A superposition of T1184R FH19-20 (yellow) with wild-type FH19-20 (green) belonging to the C3d–wild-type FH19-20 heterotrimer. (*d*) Electrostatic surface representation of C3d-2 (calculated using the *APBS* plug-in for *PyMOL*) highlighting the highly negatively (red) charged concave surface and the interacting Arg1203 (forming a salt bridge with Glu160 of C3d-2). A model of the positively charged Arg1184 (belonging to T1184R FH19-20) interacting with a region of negative charge on the surface of C3d-2 (details of the interaction are shown in Fig. 2).

**Table 2**
Reported binding affinities of wild-type FH19-20 and T1184R FH19-20 for C3b, C3dg, C3d and heparin.

| | Wild-type FH19-20 | T1184R FH19-20 | Reference |
|---|---|---|---|
| C3b | ~6 μ*M* (C3b; CM5) | ~2 μ*M* (C3b; CM5) | Ferreira *et al.* (2009)† |
| | 9.1 ± 0.4 μ*M* (C3b–biotin; SA) | ~5 μ*M* (C3b–biotin; SA) | Ferreira *et al.* (2009)† |
| | | Decrease relative to wild type | Lehtinen *et al.* (2009)‡ |
| C3dg | 3.8 ± 0.5 μ*M* (CM5) | 4.4 ± 0.2 μM (CM5) | Morgan *et al.* (2011)† |
| C3d | 6.2 ± 0.4 μ*M* (recombinant C3d; CM5) | 4.2 ± 0.1 μ*M* (recombinant C3d; CM5) | Morgan *et al.* (2011)† |
| | 8.2 ± 0.6 μ*M* (plasma C3d; CM5) | 6.8 ± 0.2 μ*M* (plasma C3d; CM5) | Morgan *et al.* (2011)† |
| | | No change relative to wild type | Lehtinen *et al.* (2009)‡ |
| Heparin | 100% (377 m*M* NaCl) | 129% (488 m*M* NaCl) | Ferreira *et al.* (2009)§ |
| | | Increase relative to wild type | Lehtinen *et al.* (2009)§ |

† $K_d$ values for FH19-20–C3 (C3b, C3dg or C3d) fragments coupled to CM5 or streptavidin (SA) sensor chips were recorded by surface plasmon resonance under physiological ionic strength buffer conditions (Ferreira *et al.*, 2009; Morgan *et al.*, 2011). ‡ Binding affinities were calculated by the relative capacity of unlabelled wild-type or T1184R forms of FH19-20 to inhibit binding of $^{125}$I-labelled FH19-20 to C3b or C3d under half physiological ionic strength buffer conditions (Lehtinen *et al.*, 2009). § Relative heparin-binding affinities of wild-type and T1184R forms of FH19-20 were recorded as a measure of the elution profile (peak maxima values given) of these recombinant proteins from heparin-conjugated beads in the presence of a linear NaCl gradient (Ferreira *et al.*, 2009; Lehtinen *et al.*, 2009).

the mutant has more widespread effects on the electrostatic properties of CCP20, as discussed below in the context of the critical C3b/self-surface recognition properties of FH.

The structure of wild-type FH19-20 in complex with C3d has recently been determined by X-ray crystallography (Morgan *et al.*, 2011), as was the structure of a functionally deficient double mutant D1119G/Q1139A of FH19-20 in complex with C3d (Kajander *et al.*, 2011). Both structure determinations identified virtually identical binding sites on C3d that can be extrapolated to the context of the physiological C3b–FH interaction (Figs. 2 and 3). Both studies demonstrated that C3b engagement by FH19-20 primarily involves residues from within CCP19, with additional contributions from residues within the cleft between the modules and the N-terminal region of CCP20 (Figs. 2 and 3; Kajander *et al.*, 2011; Morgan *et al.*, 2011). This proposed C3b-binding site on FH19-20 is supported by NMR and by binding studies with mutant proteins, many of which are linked to aHUS. Several aHUS-associated C3b missense mutations have also been identified within, or in close proximity to, this interface (Frémeaux-Bacchi *et al.*, 2008; Miller *et al.*, 2010). Engineered C3d mutants designed to interrogate this interface also result in reduced binding to FH19-20 (Kajander *et al.*, 2011; Morgan *et al.*, 2011). The current structure indicates very clearly that the T1184R mutation would have no direct effect on this binding site.

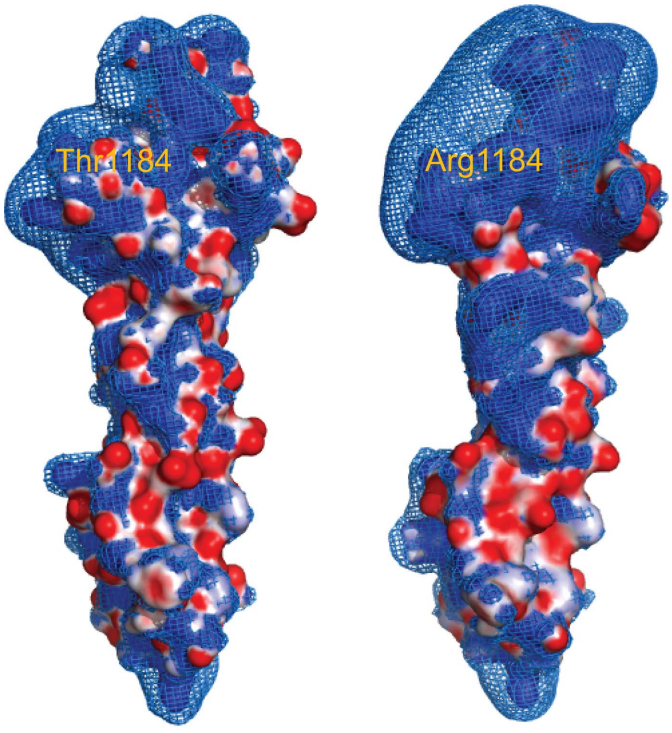


**Figure 4**
Electrostatic surface representations of (*a*) wild-type FH19-20 (PDB entry 2g7i; Jokiranta *et al.*, 2006) and (*b*) T1184R FH19-20 (PDB entry 3r62). Further indicated on both molecules as a blue mesh is a positive isosurface map contoured at +4 *kT*/*e*. The location of residue 1184, corresponding to a threonine in wild-type FH and an arginine in this aHUS-associated variant, is indicated in orange. Positively and negatively charged areas of these molecules are indicated in blue and red, respectively. This figure was generated using the *APBS* plugin for *PyMOL* (DeLano Scientific LLC). The *PDB2PQR* server was utilized to generate the PQR file used to run *APBS* (Dolinsky *et al.*, 2004).

In addition to this CCP19-dominated C3b-binding surface, a distinct interaction was observed in each of the reported C3d–FH19-20 complexes between CCP20 of FH and an additional C3d molecule; the orientation of this second C3d molecule relative to CCP20 varies between the two complexes (Fig. 3). Kajander and coworkers proposed on the basis of their structure that the formation of a physiological C3b–FH–C3d trimolecular complex may occur on the cell surface (Fig. 2). However, it is unclear how commonly such a complex would occur in a physiological setting since it would require a very specific juxtaposition of a C3b molecule (bound mainly to module 19) and an adjacent C3d molecule (bound to module 20 of the same FH molecule). Moreover, while NMR data supported the aforementioned CCP19-dominated binding site, they were not consistent with this additional CCP20-mediated interaction.

There have been three conflicting studies of the binding of T1184R FH19-20 to one or more of C3b, C3dg and C3d (Ferreira *et al.*, 2009; Lehtinen *et al.*, 2009; Morgan *et al.*, 2011). Ferreira and coworkers and Morgan and coworkers reported that a T1184R mutant exhibited increased binding relative to wild-type to C3b, with less significant increases or null changes

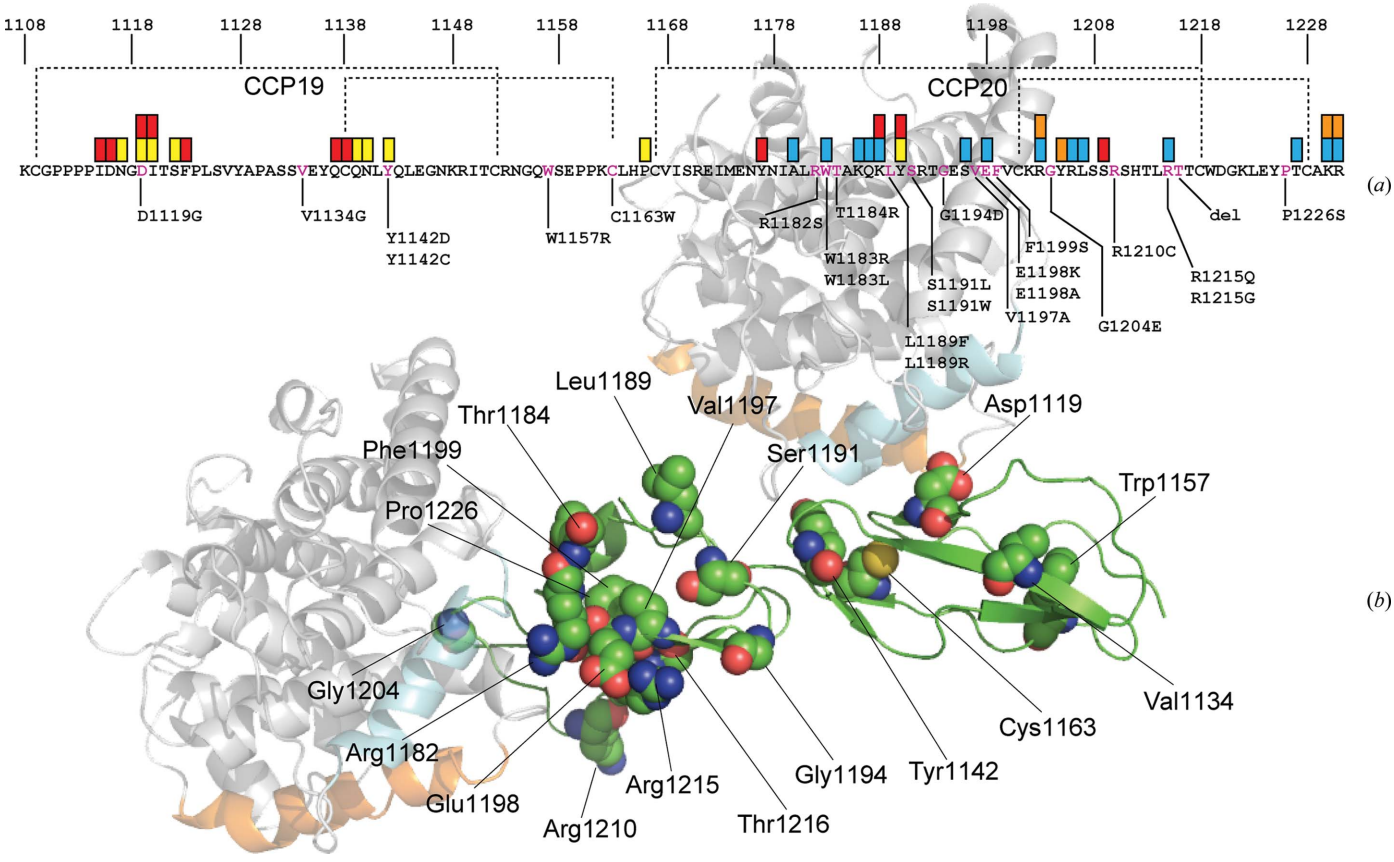


**Figure 5**
Primary sequence of wild-type FH19-20 with aHUS-associated missense and deletion mutations indicated (Saunders *et al.*, 2007). Shown in yellow are those residues which have been identified by X-ray crystallography as contributing to a C3b–FH19-20 interface (Kajander *et al.*, 2011; Morgan *et al.*, 2011). Indicated in red are those residues which have been identified by NMR line-broadening studies as being important in C3d (C3b) binding (Morgan *et al.*, 2011). Indicated in orange are residues which have been proposed to form an additional physiological C3d-binding surface (Kajander *et al.*, 2011). Indicated in blue are residues which have been identified by NMR chemical shift perturbation studies as being involved in heparin (GAG-mimetic) binding (Herbert *et al.*, 2006; Morgan *et al.*, 2011). (*b*) The C3d–wild-type FH19-20 heterotrimer, highlighting the positions of aHUS-associated missense and deletion mutations (shown as spheres).

observed for C3d and C3dg, respectively (Ferreira *et al.*, 2009; Morgan *et al.*, 2011; Table 2). In contrast, Lehtinen and coworkers reported that T1184R exhibited a decreased capacity to inhibit binding of radiolabelled wild-type FH19-20 to immobilized C3b (although no such decrease was observed for immobilized C3d; Table 2; Lehtinen *et al.*, 2009). The substitution of an arginine for a threonine has a profound effect on the electrostatics within this region and accordingly may have electrostatic steering effects (Fig. 4) that could explain any of the aforementioned binding results. Interestingly, however, when our new T1184R FH19-20 structure is modelled onto the crystal complex of C3d–FH19-20, Arg1184 appears to directly overlap with the additional putative CCP20–C3d interface (Kajander *et al.*, 2011; Figs. 2 and 3). Thus, the lack of any substantive effect of this mutation on C3d-binding (upon which all studies agree) is not consistent with the CCP20–C3d interaction observed in the crystal structure being physiologically important.

Numerous aHUS-associated missense mutations within module 20 modify the GAG-binding properties of FH19-20 (Fig. 5). Generally speaking, removing positive charge from CCP20 reduces affinity for heparin (a GAG mimetic) and for models of host-cell surfaces (Ferreira *et al.*, 2009; Lehtinen *et al.*, 2009). Specifically, positive-charge-deficient CCP20 mutants exhibit decreased binding to heparin-conjugated media (Ferreira *et al.*, 2009; Lehtinen *et al.*, 2009) and to activated mouse glomerular endothelial cells (mGEnC-1; Lehtinen *et al.*, 2009). They also have reduced capacity to inhibit binding of radiolabelled FH19-20 to C3b-coated sheep erythrocytes (Ferreira *et al.*, 2009). Conversely, the addition of positive charge increases affinity for heparin and mGEnC-1 cells (Ferreira *et al.*, 2009; Lehtinen *et al.*, 2009). For example, T1184R FH19-20 binds more strongly to a heparin-conjugated matrix than wild-type FH19-20 (Ferreira *et al.*, 2009; Lehtinen *et al.*, 2009; Table 2). In related experiments, NMR has been used to identify residues whose resonances undergo significant perturbations upon titration of the fully sulfated heparin tetrasaccharide or the octasaccharide fraction of heparin into samples of FH19-20 or the FH19-20–C3d complex, respectively (Herbert *et al.*, 2006; Morgan *et al.*, 2011; Fig. 5). The new structure shows that T1184R extends an electropositive region of CCP20 that has previously been implicated by NMR in GAG binding (Figs. 4 and 5). This is then consistent with a model in which T1184R enhances binding between module 20

and cell-surface GAGs, thereby disturbing the fine balance of interactions needed to ensure that an FH molecule functions effectively when confronted with multiple C3b molecules tethered to a self-surface.

In conclusion, the disease-associated T1184R mutation perturbs neither the structure of FH nor its primary C3b-interaction site. The location of this mutation would overlap with a putative CCP20–C3d interaction observed in crystal structures, but in fact has no effect on C3d binding. It is likely to contribute to the development of aHUS by significantly altering the GAG-binding properties of the C-terminal module of FH, although perturbation of an additional putative C3d-binding site cannot be ruled out on the basis of these data.

Use of the Protein Production Facilities at the University of Edinburgh was supported by The Wellcome Trust, the Scottish University Life Sciences Alliance and the BBSRC. APH was supported by Wellcome Trust grant No. 078780/Z/05/Z (to DU and PNB). Funding for this project was provided by the School of Biological Sciences at the University of Edinburgh to JPH.

## References

Aslam, M. & Perkins, S. J. (2001). *J. Mol. Biol.* **309**, 1117–1138.
Bhattacharjee, A., Lehtinen, M. J., Kajander, T., Goldman, A. & Jokiranta, T. S. (2010). *Mol. Immunol.* **47**, 1686–1691.
Blackmore, T. K., Hellwage, J., Sadlon, T. A., Higgs, N., Zipfel, P. F., Ward, H. M. & Gordon, D. L. (1998). *J. Immunol.* **160**, 3342–3348.
Blackmore, T. K., Sadlon, T. A., Ward, H. M., Lublin, D. M. & Gordon, D. L. (1996). *J. Immunol.* **157**, 5422–5427.
Caprioli, J., Castelletti, F., Bucchioni, S., Bettinaglio, P., Bresin, E., Pianetti, G., Gamba, S., Brioschi, S., Daina, E., Remuzzi, G. & Noris, M. (2003). *Hum. Mol. Gen.* **12**, 3385–3395.
Chen, V. B., Arendall, W. B., Headd, J. J., Keedy, D. A., Immormino, R. M., Kapral, G. J., Murray, L. W., Richardson, J. S. & Richardson, D. C. (2010). *Acta Cryst.* D**66**, 12–21.
Córdoba, S. R. de & de Jorge, E. G. (2008). *Clin. Exp. Immunol.* **151**, 1–13.
Dolinsky, T. J., Nielsen, J. E., McCammon, J. A. & Baker, N. A. (2004). *Nucleic Acids Res.* **32**, W665–W667.
Emsley, P. & Cowtan, K. (2004). *Acta Cryst.* D**60**, 2126–2132.
Ferreira, V. P., Herbert, A. P., Cortés, C., McKee, K. A., Blaum, B. S., Esswein, S. T., Uhrín, D., Barlow, P. N., Pangburn, M. K. & Kavanagh, D. (2009). *J. Immunol.* **182**, 7009–7018.
Frémeaux-Bacchi, V. *et al.* (2008). *Blood*, **112**, 4948–4952.
Gordon, D. L., Kaufman, R. M., Blackmore, T. K., Kwong, J. & Lublin, D. M. (1995). *J. Immunol.* **155**, 348–356.
Herbert, A. P., Deakin, J. A., Schmidt, C. Q., Blaum, B. S., Egan, C., Ferreira, V. P., Pangburn, M. K., Lyon, M., Uhrín, D. & Barlow, P. N. (2007). *J. Biol. Chem.* **282**, 18960–18968.
Herbert, A. P., Uhrín, D., Lyon, M., Pangburn, M. K. & Barlow, P. N. (2006). *J. Biol. Chem.* **281**, 16512–16520.
Jokiranta, T. S., Jaakola, V. P., Lehtinen, M. J., Pärepalo, M., Meri, S. & Goldman, A. (2006). *EMBO J.* **25**, 1784–1794.
Kajander, T., Lehtinen, M. J., Hyvärinen, S., Bhattacharjee, A., Leung, E., Isenman, D. E., Meri, S., Goldman, A. & Jokiranta, T. S. (2011). *Proc. Natl Acad. Sci. USA*, **108**, 2897–2902.
Kavanagh, D., Goodship, T. H. & Richards, A. (2006). *Brit. Med. Bull.* **77–78**, 5–22.
Krissinel, E. & Henrick, K. (2007). *J. Mol. Biol.* **372**, 774–797.
Lehtinen, M. J., Rops, A. L., Isenman, D. E., van der Vlag, J. & Jokiranta, T. S. (2009). *J. Biol. Chem.* **284**, 15650–15658.
McCoy, A. J., Grosse-Kunstleve, R. W., Adams, P. D., Winn, M. D., Storoni, L. C. & Read, R. J. (2007). *J. Appl. Cryst.* **40**, 658–674.
Meri, S. & Pangburn, M. K. (1994). *Biochem. Biophys. Res. Commun.* **198**, 52–59.
Miller, E. C., Roumenina, L., Fremeaux-Bacchi, V. & Atkinson, J. P. (2010). *Mol. Immunol.* **47**, 2291.
Morgan, H. P., Schmidt, C. Q., Guariento, M., Blaum, B. S., Gillespie, D., Herbert, A. P., Kavanagh, D., Mertens, H. D. T., Svergun, D. I., Uhrín, D., Johansson, C. M., Barlow, P. N. & Hannan, J. P. (2011). *Nature Struct. Mol. Biol.* **18**, 463–470.
Murshudov, G. N., Skubák, P., Lebedev, A. A., Pannu, N. S., Steiner, R. A., Nicholls, R. A., Winn, M. D., Long, F. & Vagin, A. A. (2011). *Acta Cryst.* D**67**, 355–367.
Pangburn, M. K. (2000). *Immunopharmacology*, **49**, 149–157.
Pangburn, M. K. (2002). *J. Immunol.* **169**, 4702–4706.
Pangburn, M. K., Atkinson, M. A. & Meri, S. (1991). *J. Biol. Chem.* **266**, 16847–16853.
Pangburn, M. K., Schreiber, R. D. & Müller-Eberhard, H. J. (1977). *J. Exp. Med.* **146**, 257–270.
Richards, A., Buddles, M. R., Donne, R. L., Kaplan, B. S., Kirk, E., Venning, M. C., Tielemans, C. L., Goodship, J. A. & Goodship, T. H. (2001). *Am. J. Hum. Genet.* **68**, 485–490.
Saunders, R. E., Abarrategui-Garrido, C., Frémeaux-Bacchi, V., Goicoechea de Jorge, E., Goodship, T. H., López Trascasa, M., Noris, M., Ponce Castro, I. M., Remuzzi, G., Rodríguez de Córdoba, S., Sánchez-Corral, P., Skerka, C., Zipfel, P. F. & Perkins, S. J. (2007). *Hum. Mutat.* **28**, 222–234.
Schmidt, C. Q., Herbert, A. P., Kavanagh, D., Gandy, C., Fenton, C. J., Blaum, B. S., Lyon, M., Uhrín, D. & Barlow, P. N. (2008). *J. Immunol.* **181**, 2610–2619.
Sharma, A. K. & Pangburn, M. K. (1996). *Proc. Natl Acad. Sci. USA*, **93**, 10996–11001.
Venables, J. P., Strain, L., Routledge, D., Bourn, D., Powell, H. M., Warwicker, P., Diaz-Torres, M. L., Sampson, A., Mead, P., Webb, M., Pirson, Y., Jackson, M. S., Hughes, A., Wood, K. M., Goodship, J. A. & Goodship, T. H. (2006). *PLoS Med.* **3**, e431.
Warwicker, P., Goodship, T. H., Donne, R. L., Pirson, Y., Nicholls, A., Ward, R. M., Turnpenny, P. & Goodship, J. A. (1998). *Kidney Int.* **53**, 836–844.
Weiler, J. M., Daha, M. R., Austen, K. F. & Fearon, D. T. (1976). *Proc. Natl Acad. Sci. USA*, **73**, 3268–3272.
Whaley, K. & Ruddy, S. (1976). *J. Exp. Med.* **144**, 1147–1163.
Wu, J., Wu, Y.-Q., Ricklin, D., Janssen, B. J., Lambris, J. D. & Gros, P. (2009). *Nature Immunol.* **10**, 728–733.
Zipfel, P. F., Jokiranta, T. S., Hellwage, J., Koistinen, V. & Meri, S. (1999). *Immunopharmacology*, **42**, 53–60.